https://doi.org/10.5194/egusphere-2026-3098
Preprint. Discussion started: 23 June 2026

Reassessing the Permafrost Carbon Feedback: The Decisive Role of Dynamic Vegetation

Thomas Kleinen[1], Helena Bergstedt[2], Philipp de Vrese[1], Tobias Stacke[1], and Victor Brovkin[1]

[1]Max Planck Institute for Meteorology, Bundesstr. 53, 20146 Hamburg, Germany
[2]b.geos, Industriestr. 1, 2100 Korneuburg, Austria

Correspondence: Thomas Kleinen (thomas.kleinen@mpimet.mpg.de)

Abstract. The permafrost region stores $\sim 1300\,\mathrm{PgC}$, and its response to warming is a significant uncertainty in future climate projections. We assess how the treatment of vegetation dynamics and CO_2 fertilisation influences the permafrost carbon feedback (PCF) by performing experiments with the land-surface model ICON-Land. A vertically explicit implementation of the YASSO soil-carbon scheme resolves depth-dependent carbon pools, as well as temperature and moisture controls on decomposition, while a newly introduced cold-adapted shrub plant-functional type (PFT) enables a more realistic description of Arctic vegetation.

Using CMIP5-derived climate forcing, we performed nine offline experiments from the year 2020 to 2299 CE under RCP 2.6, 4.5 and 8.5. The experiments isolate the effects of (a) climate warming with fixed 2019 CO_2 and vegetation, (b) rising CO_2 with constant vegetation cover, and (c) the effects of both rising CO_2 and a fully dynamic vegetation. All simulations start from a data-constrained pre-industrial permafrost soil carbon inventory.

When vegetation is held static, strong warming (RCP 8.5) alone drives a loss of $\sim 650\,\mathrm{PgC}$ by 2300 CE, turning the permafrost region from a modest sink of carbon into a strong source. Allowing CO_2 fertilisation but no vegetation change reduces the loss to $\sim 250\,\mathrm{PgC}$ because enhanced NPP increases litter inputs. In the fully dynamic experiments, shrubification and northward tree expansion dramatically increase aboveground biomass (of up to $199\,\mathrm{PgC}$) and litterfall, limiting soil-C loss to only $\sim 70\,\mathrm{PgC}$. Consequently, total permafrost-region carbon declines by $< 100\,\mathrm{PgC}$ under RCP 8.5 and even shows a net gain under the low-emission pathways (RCPs 2.6 and 4.5).

These results demonstrate that the sign and magnitude of the PCF are highly sensitive to the representation of vegetation dynamics. Dynamic competition among PFTs, CO_2-driven NPP enhancement, and the resulting shifts in carbon accumulation together can offset most of the carbon released by thawing soils. Incorporating realistic Arctic vegetation, especially cold-tolerant shrubs, is therefore decisive for reliable projections of the permafrost carbon feedback and its impact on the global carbon cycle.

1 Introduction

The Arctic permafrost region is one of the most critical regions in the global carbon (C) cycle, as it contains a vast reservoir of organic matter accumulated under cold conditions over millennia. Covering approximately 15% of the Northern Hemisphere

https://doi.org/10.5194/egusphere-2026-3098
Preprint. Discussion started: 23 June 2026

(NH) land area (Obu, 2021), permafrost soils are estimated to contain about $1300\,\mathrm{PgC}$ (uncertainty range: $1100-1500\,\mathrm{PgC}$), of which $1035\pm150\,\mathrm{PgC}$ are located within the upper three metres (Hugelius et al., 2014). This stock is nearly double the amount of carbon currently contained in the atmosphere and exceeds the total carbon stored in living biomass globally (Schuur et al., 2015, 2022). Under current climatic conditions, a significant portion of this carbon remains preserved due to low temperatures and frozen conditions that strongly inhibit microbial decomposition. However, the stability of this reservoir is increasingly precarious. The Arctic is warming three to four times faster than the global mean temperature due to Arctic Amplification (Rantanen et al., 2022; Zhou et al., 2024). This rapid warming drives permafrost degradation, increasing the thickness of the active layer (Romanovsky et al., 2017). As previously frozen organic matter becomes accessible to microbial decomposition, there is a substantial risk of large-scale carbon release, potentially creating a positive feedback loop that accelerates global climate change (Schuur et al., 2015).

The magnitude of this permafrost carbon feedback (PCF) has been a focal point of climate research for over a decade. Early estimates suggested a potentially catastrophic release of carbon, though subsequent refinements have constrained the uncertainty. Schaefer et al. (2011) provided one of the first comprehensive assessments, estimating that permafrost thaw could release $190\pm64\,\mathrm{PgC}$ by 2200 CE, depending on the warming scenario. Since then, Earth System Models (ESMs) have increasingly incorporated permafrost processes to better quantify these feedbacks. Koven et al. (2011) demonstrated, using the ORCHIDEE land surface model, that including vertical soil biogeochemistry and permafrost dynamics significantly alters projected carbon fluxes compared to models lacking these features. Similarly, Koven et al. (2015) highlighted that carbon losses from permafrost regions are governed by dynamics of deep decomposition processes. These studies established the necessity of representing frozen soil processes explicitly in climate models.

Despite these advancements, significant discrepancies remain between models. Ensemble studies and intercomparison projects have been instrumental in diagnosing these uncertainties. Burke et al. (2017b) quantified the uncertainties of permafrost carbon-climate feedbacks across an ensemble of climate changes with climate change patterns from several models, as well as two land surface models, finding that while there is a net release of carbon in all cases, the amount varies by an order of magnitude. This variability stems from differences in soil carbon decomposition parameterisations, and the representation of soil thermal dynamics. McGuire et al. (2016) further elaborated on this variability in a model intercomparison focused on permafrost carbon dynamics, noting that the treatment of snow insulation, soil column depth, treatment of disturbances, and the sensitivity of carbon assimilation to atmospheric CO_2 are important drivers of divergence among models. However, a common limitation in many previous assessments of the PCF is the treatment of vegetation response to warming and elevated CO_2.

The interaction between soil thaw and vegetation growth is complex: warming extends the growing season and improves thermal conditions for plant growth, while elevated CO_2 concentrations can enhance photosynthetic rates and water-use efficiency, a phenomenon known as CO_2 fertilisation (Ainsworth and Long, 2005). Observational evidence over the past few decades indicates a widespread "greening" of the Arctic, characterised by increased biomass and productivity (Frost et al., 2025). A prominent feature of this change is "shrubification", where shrubs expand into areas previously dominated by graminoids or bare ground (Sturm et al., 2001; Tape et al., 2006; Myers-Smith et al., 2011). Shrubs alter the local microclimate by trapping snow, which insulates the soil in winter, and by modifying surface albedo. Furthermore, there is evidence suggesting a north-

https://doi.org/10.5194/egusphere-2026-3098
Preprint. Discussion started: 23 June 2026

ward shift of the boreal treeline, reminiscent of vegetation patterns during the warmer early Holocene (Bigelow et al., 2003; Williams, 2003), although recent observational constraints on this shift remain controversial (Rotbarth et al., 2023, 2025; Feng et al., 2026).

These vegetation changes imply a potential increase in carbon uptake and storage in biomass and litter, which could partially or fully offset carbon losses from thawing soils. However, the representation of these dynamics in ESMs is often inadequate. Many models do not consider the changes in vegetation distribution with climate change, and those that do tend to lack adequate plant functional types (PFTs) for representing vegetation in the Arctic. Especially shrubs are often neglected, leading to an underestimation of woody biomass expansion (Kaplan et al., 2003).

Uncertainty in the net carbon balance of the permafrost region thus stems largely from the interplay between soil carbon losses and vegetation carbon gains. If vegetation dynamics are neglected, models may project the high latitudes as a strong carbon source. However, if vegetation is allowed to adapt dynamically to changing climatic and atmospheric conditions, the region might remain a neutral sink or even strengthen its sink capacity. We attempted a previous assessment of the role of vegetation in the PCF, in Kleinen and Brovkin (2018) we analysed the effects of climate change and CO_2 on the permafrost carbon cycle, including the vegetation component. We showed that the permafrost region carbon cycle impact on atmospheric CO_2 is substantially reduced by increased uptake through vegetation. However, our analysis largely focused on the soil carbon storage and neglected to explicitly investigate the impact of changes in vegetation distribution. Furthermore, the dynamic vegetation scheme we used at the time was lacking a shrub PFT adequate for the Arctic, thus potentially underestimating carbon accumulation effects. Thus, the interaction between permafrost-appropriate soil carbon schemes and dynamic vegetation remains underexplored in the context of long-term climate change scenarios.

To address this gap, we utilise the land surface model ICON-Land, coupled with the JSBACH4 vegetation and biogeochemistry module. We implement a vertically explicit version of the YASSO soil carbon model (Liski et al., 2005; de Vrese et al., 2021) and enhance the dynamic vegetation scheme with a cold-adapted shrub PFT to better represent Arctic vegetation competition (Kaplan et al., 2003). We perform a series of experiments extending to the year 2300 CE under different Representative Concentration Pathways (RCPs). By systematically varying the treatment of atmospheric CO_2 concentrations and vegetation dynamics, we isolate the contributions of climate warming, CO_2 fertilisation, and vegetation composition changes to the permafrost region carbon balance. We hypothesise that accounting for dynamic vegetation responses, particularly shrubification and tree line expansion, significantly mitigates projected soil carbon losses. Our results suggest that the representation of vegetation dynamics is a decisive factor in determining whether the high latitudes act as a source or a sink of carbon in a warming world. The following sections describe the model configuration and experimental design, present the results of the scenario simulations, and discuss the implications for the global carbon cycle and future climate projections.

2 Model, experiments and data

We use the land surface model ICON-Land, coupled with the JSBACH4 vegetation and biogeochemistry module (Schneck et al., 2022). JSBACH4 is based on the JSBACH model (Brovkin et al., 2009; Reick et al., 2013; Goll et al., 2015; Reick et al.,

https://doi.org/10.5194/egusphere-2026-3098
Preprint. Discussion started: 23 June 2026

2021) developed for MPI-ESM (Mauritsen et al., 2019), and thus shares much of the model physics and biogeochemistry with its predecessor.

2.1 Soil carbon model YASSO

JSBACH4 uses the soil carbon model YASSO (Liski et al., 2005; Tuomi et al., 2009, 2011; Goll et al., 2015). As implemented in JSBACH (Goll et al., 2015), YASSO considers soil organic matter (SOM) as carbon solubility fractions, separating litter C in acid soluble (A), water soluble (W), ethanol soluble (E) and non-soluble (N) fractions to define the separate carbon pools. We distinguish between above- and belowground litter, such that the pools exist for each of these locations. Below the surface, an additional humus pool contains carbon that decomposes on long timescales. Finally, green and woody litter are considered separately, both requiring their own pool structure.

Each of these SOM pools C_i is decomposed in a first order differential equation $\frac{d}{dt}C_i = k\gamma_i C_i$, with decomposition rates dependent on a pool-dependent rate constant γ_i, modulated by an environmental factor k. For the YASSO model (Tuomi et al., 2008, 2009, 2011), the rate constants γ_i have been determined from a large number of litter bag experiments, and k has been determined from a regression onto annual mean surface air temperature and annual total precipitation. Thus, $k = \exp\left(\beta_1 T + \beta_2 T^2\right) \cdot (1 - \exp\left[\kappa P\right])$ with T annual mean surface air temperature and P annual total precipitation, $\beta_1 = 0.095\,^\circ C^{-1}$, $\beta_2 = -0.0014\,^\circ C^{-2}$, and $\kappa = -1.21$ (Tuomi et al., 2008, 2009; Goll et al., 2015).

In its original form, the YASSO model is not well suited to modelling carbon in the permafrost region, as it is zero-dimensional, not taking a belowground vertical dimension into account, and thus unable to distinguish between thawed soil at the top of the soil column and frozen soil further down. Furthermore, SOM decomposition is solely dependent on environmental conditions above the soil, and therefore unable to consider different physical conditions at depth.

In order to remedy this shortcoming, we follow de Vrese et al. (2021) by extending the YASSO model vertically. In our improved vertically explicit implementation, the treatment of the aboveground litter remains unchanged, but the belowground litter and humus pools become depth-dependent by replicating them for each soil layer. Furthermore, the environmental factor k is changed to a vertically explicit formulation, with k_l, the environmental modification factor for layer l, taking into account layer temperature T_l and layer moisture w_l. In full, k_l is formulated multiplicatively

$$k_l = d_{T,l} \cdot d_{W,l} \tag{1}$$

taking into account a soil temperature dependent modifier $d_{T,l}$ and a soil moisture dependent modifier $d_{W,l}$. Here we are using

$$d_{T,l} = \exp\left(\beta_1 T_l + \beta_2 T_l^2\right) \tag{2}$$

as the temperature modifier with $\beta_1 = 0.095\,^\circ C^{-1}$ and $\beta_2 = -0.0014\,^\circ C^{-2}$, as in (Goll et al., 2015), but for temperature T_l on soil layers l instead of the near surface air temperature. For the soil moisture dependence of decomposition, we generally

https://doi.org/10.5194/egusphere-2026-3098
Preprint. Discussion started: 23 June 2026

follow the approach in the CENTURY model (Kelly et al., 2000), using

$$d_{W,l} = \left(\frac{w_l^* - b}{a - b}\right)^{d\frac{b-a}{a}} \cdot \left(\frac{w_l^*}{a}\right)^d \tag{3}$$

as the soil moisture-dependent modifier, with $a = 0.575$, $b = 1.5$, and $d = 3$, as well as a soil moisture w_l^* representing the relative saturation of the soil, only considering liquid water.

2.2 Carbon input and vertical transport

The YASSO soil carbon model receives carbon inputs from litterfall. 70% of the woody litter and 50% of the green litter generated by the vegetation are considered as belonging to the aboveground litter pool, with the remainder considered belowground litter. While the aboveground litterfall is added to the aboveground litter pools directly, the belowground litterfall is distributed to the soil layers according to the vertical distribution of roots, where we assume a root distribution according to Jackson et al. (1996).

Transport between soil layers is considered as a diffusion problem following de Vrese et al. (2021) and Burke et al. (2017a), with a constant diffusivity representing bioturbation in non-permafrost areas, while a diffusivity dependent on soil conditions represents cryoturbation in permafrost regions. In non-permafrost regions, we assume a diffusivity of $1.5\,\mathrm{cm^2 yr^{-1}}$ at the surface, decreasing linearly with depth down to either $3\,\mathrm{m}$ or bedrock depth. In permafrost regions, we assume a diffusivity of up to $15\,\mathrm{cm^2 yr^{-1}}$, scaled by the active layer saturation and a representation of freeze-thaw cycles.

Finally, aboveground litter is not redistributed vertically via bio- or cryoturbation. In order to prevent an excessive accumulation of organic matter at the surface, aboveground C that excceeds a threshold organic matter density of $75\,\mathrm{kgC\,m^{-3}}$(Chojnacky et al., 2009; O'Donnell et al., 2009) is mixed into the topmost soil layer carbon. Likewise, belowground C that exceeds a threshold of $150\,\mathrm{kgC\,m^{-3}}$ – e.g. if the mixing by bio- and cryoturbation is not efficient enough – is mixed into the soil level below.

2.3 Shrubs in the dynamical vegetation

As the DYNVEG dynamical vegetation module (Brovkin et al., 2013; Reick et al., 2013, 2021) implemented in JSBACH4 does not contain shrub PFTs suitable for Arctic regions, we added an additional shrub PFT to JSBACH, based on Kaplan et al. (2003).

PFTs in JSBACH generally compete through their net primary productivity (NPP), with PFTs with higher NPP establishing in uncolonised land faster than PFTs with lower NPP (Reick et al., 2013). Furthermore, woody PFTs have an advantage over non-woody PFT, albeit with slower growth due to their requirement of stem growth. Thus, grasses move into uncolonised land first, to be later replaced by woody PFTs. Finally, disturbances (wind throw, fire, mortality) remove PFTs, opening up land for new colonisation.

JSBACH PFTs are also subject to bioclimatic limits, considering physiological requirements by PFTs, for example frost-free conditions required by tropical trees. In its basic form, DYNVEG contains 8 natural PFTs: Two tropical tree PFTs, two extratropical tree PFTs, two grass PFTs, and two shrub PFTs. While these natural PFTs generally cover the globe well, there is

https://doi.org/10.5194/egusphere-2026-3098
Preprint. Discussion started: 23 June 2026

one exception: Arctic vegetation is not represented as well as vegetation in other areas, as the existing shrub PFTs do not thrive under Arctic conditions.

Following Kaplan et al. (2003), we thus implement a PFT representing shrubs adapted to the cold conditions of the Arctic. For simplicity, we model these shrubs on an evergreen phenology, thus resembling extratropical evergreen trees in many respects, but with a maximum height of $1.0\,\mathrm{m}$. In terms of bioclimatic limits, the maximum temperature of the coldest month is $TC_{max} = -2.0\,^{\circ}\mathrm{C}$, the maximum temperature of the warmest month is $TW_{max} = 18\,^{\circ}\mathrm{C}$ and the shrubs need minimum growing degree days $GDD_{min} = 250\,^{\circ}\mathrm{C\,d}$, and a minimum winter snow height $S_{min} = 0.2\,\mathrm{m}$. The choice of the underlying evergreen phenology is purely pragmatic, as the evergreen trees in JSBACH grow in a somewhat larger environmental envelope than deciduous trees. The new PFT, however, is intended to be representative of both evergreen and deciduous cold shrubs, and it then competes with the other PFTs in the dynamical vegetation scheme (Reick et al., 2013).

2.4 Model configuration and experiments

We perform model experiments on a global triangular grid in resolution R2B4, corresponding to an average grid spacing of roughly $160\,\mathrm{km}$. The land surface model resolves 11 vertical soil layers of variable thickness, ranging from $6.25\,\mathrm{cm}$ for the topmost layer to $26.74\,\mathrm{m}$ for the lowest soil layer, with the lower boundary of the soil column at $50\,\mathrm{m}$. This is quite different from the model's standard vertical resolution of 5 layers resolving the ground until a depth of $\sim 10\,\mathrm{m}$, with the increased vertical discretization being required to better capture the vertical mixing, especially of carbon, and the increased column depth allowing for a better representation of near-surface soil warming (García-Pereira et al., 2025).

We run the model in an offline configuration, forced by climate model output obtained from the experiments performed with the Max Planck Institute for Meteorology Earth System Model MPI-ESM (Giorgetta et al., 2013) for Phase 5 of the Coupled Model Intercomparison Project (CMIP5), as no CMIP6 output from MPI-ESM is available for the extended scenario period until the year 2300 CE, and the CMIP7 experiments with ICON-XPP have not been published yet. From the CMIP5 experiments, we use the preindustrial (PI) control experiment for a model spinup under PI conditions, followed by the historical and scenario experiments. For future climate conditions, we perform three scenario experiments following the scenarios RCP 2.6, RCP 4.5 and RCP 8.5 in their extension to the year 2300 CE (Meinshausen et al., 2011). By 2299 CE, these extended scenarios lead to a warming of 1.2, 3.2, and $10.5\,\mathrm{K}$, respectively, in comparison to preindustrial. As the CMIP5 historical period ends in 2005, we extend the historical experiment to 2019 by substituting the years 2006-2019 from the RCP 4.5 experiment. For these years the difference to the RCP 2.6 and RCP 8.5 experiments is very small, and it allows starting the experiments from a point in time more in line with available reference and validation data.

In order to investigate the future carbon cycling in the permafrost region, we perform a set of nine scenario experiments. These are initialised as follows: We perform a model spinup, forced with PI control conditions, initialising the model in year 1010 CE. In year 1400 CE, we initialise the permafrost region carbon pools from observations, as described below, continuing the model spinup with PI control boundary conditions until 1849. Subsequently, we perform a historical experiment from 1850 to 2019 CE, using the CMIP5 historical forcing for 1850-2005, and the CMIP5 RCP 4.5 forcing for 2006-2019. Based on the final state of the historical experiment, we perform scenario experiments forced with RCP 2.6, RCP 4.5 and RCP

https://doi.org/10.5194/egusphere-2026-3098
Preprint. Discussion started: 23 June 2026

Table 1. Model experiments performed.

Name	climate forcing	start	end	CO_2[ppm] photosynthesis	vegetation
spinup	PI control	1010	1849	280	dynamic
permafrost-init	PI control	1400	1849	280	dynamic
historical	historical	1850	2019	historical	dynamic
con26	RCP 2.6	2020	2299	409	fixed 2019
con45	RCP 4.5	2020	2299	409	fixed 2019
con85	RCP 8.5	2020	2299	409	fixed 2019
fix26	RCP 2.6	2020	2299	RCP 2.6	fixed 2019
fix45	RCP 4.5	2020	2299	RCP 4.5	fixed 2019
fix85	RCP 8.5	2020	2299	RCP 8.5	fixed 2019
dyn26	RCP 2.6	2020	2299	RCP 2.6	dynamic
dyn45	RCP 4.5	2020	2299	RCP 4.5	dynamic
dyn85	RCP 8.5	2020	2299	RCP 8.5	dynamic

8.5 from 2020 to 2299. In order to assess the factors affecting the permafrost region carbon balance, we perform a total of nine scenario experiments: one set of three scenario experiments where increases in carbon dioxide concentration after 2019 only affect climate, but not photosynthesis, and vegetation distribution is fixed at 2019 conditions (the 'con' series, labelled con26, con45 and con85 for scenarios RCP 2.6, RCP 4.5 and RCP 8.5, respectively) to determine the baseline effect of climate change on the permafrost region carbon balance while neglecting CO_2 fertilisation and vegetation changes. A second set consists of experiments with variable CO_2 concentration following the extended CMIP5 scenarios, but with fixed 2019 vegetation distribution (the 'fix' series of experiments) to determine the effect of a rising CO_2 concentration under the present-day vegetation distribution. Finally, a third set of three scenario experiments, where CO_2 follows the extended CMIP5 scenario, and vegetation is able to adapt dynamically to the changed climatic conditions (the 'dyn' series of experiments). All experiments are summarised in Table 1. Analyses shown are performed on decadal mean states, where we mostly compare the model state of the decade 2020-2029 ('2020s') with the model state of the decade 2290-2299 ('2290s').

2.5 Permafrost C initialisation

We initialise the permafrost region soil C pools from the Northern Circumpolar Soil Carbon Database (NCSCDv2), as published in Hugelius et al. (2014). They estimate a total C stock of about $1300\,\mathrm{PgC}$ in the northern circumpolar region, with $1035 \pm 150\,\mathrm{PgC}$ at depths up to $3\,\mathrm{m}$, the depth range considered in our experiments. The NCSCDv2 contains estimates of carbon content in four depth ranges, $0-30\,\mathrm{cm}$, $0-100\,\mathrm{cm}$, $100-200\,\mathrm{cm}$, and $200-300\,\mathrm{cm}$. Using the $0.5°$ version of the NCSCDv2, we interpolate these depth ranges to our soil layers and perform a conservative remapping onto the R2B4 grid used in our model. Generally, the soil depth accessible to water and carbon is limited by a bedrock depth (Hagemann and Stacke, 2015), based on FAO (2003). In those locations where Hugelius et al. (2014) show carbon pools deeper than the FAO (2003)

https://doi.org/10.5194/egusphere-2026-3098
Preprint. Discussion started: 23 June 2026

bedrock depth, we adjust the bedrock depth to $3\,\mathrm{m}$ in order to accommodate the deeper carbon storage. When initialising the model carbon pools, we assume that (1) the distribution of PFTs reached after the initial model spinup is representative for the permafrost region, (2) the woody litter carbon pools are much less important than the ones for green litter in the permafrost region, and (3) the proportions of the various soil C pools are representative. Thus, we allocate the C from the NCSCDv2 to the green litter C pools in YASSO, with pool proportions and PFT distribution as at the end of the spinup experiment .

The original NCSCDv2 data set at $0.5°$ resolution contains $1148\,\mathrm{PgC}$ as total soil carbon in the permafrost zone. After conservative remapping, $1149\,\mathrm{PgC}$ remain in the ICON native R2B4 grid, and of these $1072\,\mathrm{PgC}$ remain on glacier-free land when considering the grid, land-sea mask and glacier mask used in our experiments. Finally, considering the model state under 1850 preindustrial conditions, $991\,\mathrm{PgC}$ are located in the zone of continuous permafrost, of which $527\,\mathrm{PgC}$ are in the unfrozen active layer, while $463\,\mathrm{PgC}$ are in the permanently frozen soil layers below the active layer.

2.6 Arctic land cover reference data

Generally, the ESA Climate Change Initiative (CCI) Land Cover product (C3S CDS, 2019; Defourny et al., 2017; Harper et al., 2023) provides a well curated global land cover product at $300\,\mathrm{m}$ resolution. For high latitude regions, however, the accuracy of the ESA CCI land cover classification is strongly reduced (Palmtag et al., 2022). Bartsch et al. (2024a) therefore derived Arctic land cover from Sentinel-1 and Sentinel-2 remote sensing data at very high resolution ($10\,\mathrm{m}$) and developed a land cover classification improving especially on the representation of wetness in the landscape, as well as the coverage with small shrubs. We merge the resulting data product (Bartsch et al., 2024b), the Circumarctic Land cover Units (CALU) data set, with the ESA CCI Land Cover product (C3S CDS, 2019) in order to obtain a land cover estimate applicable to both high and low latitudes. As shrub coverage is especially important in high latitude areas, the merged ESACCI-CALU data set is designed to be a significant improvement over the original ESACCI.

3 Results

3.1 Arctic vegetation coverage

We have evaluated the underlying dynamical vegetation module in its implementation in MPI-ESM (Reick et al., 2013), not just for modern climate states, but also for past climate states reaching back to the last glacial (Dallmeyer et al., 2021, 2023; Li et al., 2025). For the high latitudes, our extended version described above is more relevant. In comparison to the ESACCI-CALU remote sensing data, we see that the model underestimates tree cover in north-western Canada and Siberia (Figure 1). The latter is due to the fact that tree cover in Siberia is dominated by larch trees, i.e., deciduous needleleaf trees. These trees are not captured well by our vegetation dynamics, as we do not have a dedicated plant functional type (PFT). Conditions in Siberia are very cold and dry, and thus severly restricting tree growth, very much limiting productivity in our model. In north-western Canada, on the other hand, temperatures are too cold for the establishment of trees, as the growing degree days fall below the defined bioclimatic limit.

https://doi.org/10.5194/egusphere-2026-3098
Preprint. Discussion started: 23 June 2026

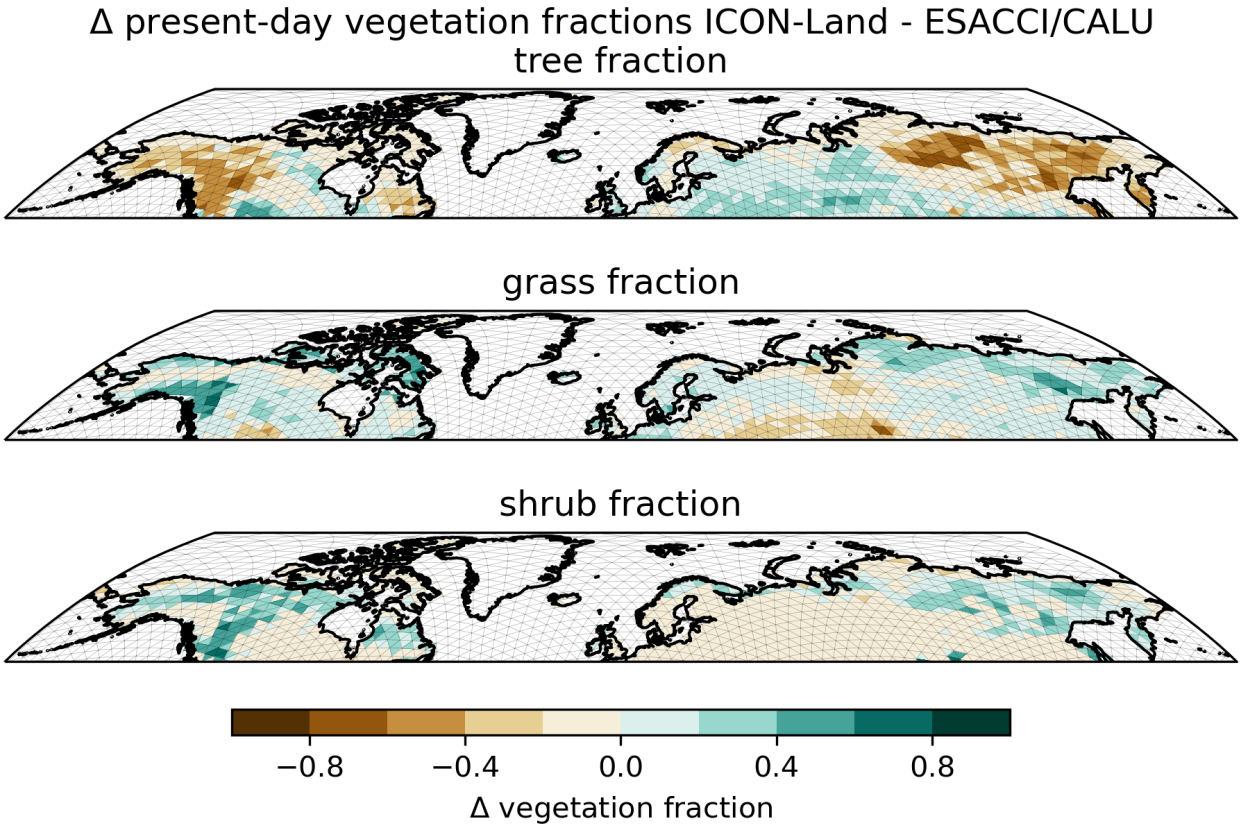

Figure 1. Difference in high latitude vegetation cover fraction for trees, grasses and shrubs: Difference between ICON-Land and ESACCI-CALU for the present (mean over 2010-2019).

The differences in the grass fraction are opposite to the differences in the tree fraction: Grasses tend to be overestimated where trees are underestimated. Shrub coverage, finally is captured reasonably well, with only small overestimates in Siberia and Alaska, while the overestimate in western Canada is slightly larger. Overall, the present-day distribution of high latitude vegetation is captured reasonably well.

3.2 Permafrost C storage

After an initial model spinup of 400 years duration, we initialise the permafrost region soil carbon pools by assimilating the Hugelius et al. (2014) permafrost region carbon stock estimate, as described above. In order to ensure equilibration of carbon state with respect to modelled processes and climate, we continue the model spinup for a further 450 years, until a simulated preindustrial state corresponding to the year 1850 is reached. During this extended spinup, carbon in frozen soil layers changes only minimally, while carbon in non-frozen soil layers in the permafrost region decreases by 199 PgC. In terms of concrete numbers, our data-constrained preindustrial estimate of carbon stocks consists of a total of 763 PgC in the (model-estimated)

https://doi.org/10.5194/egusphere-2026-3098
Preprint. Discussion started: 23 June 2026

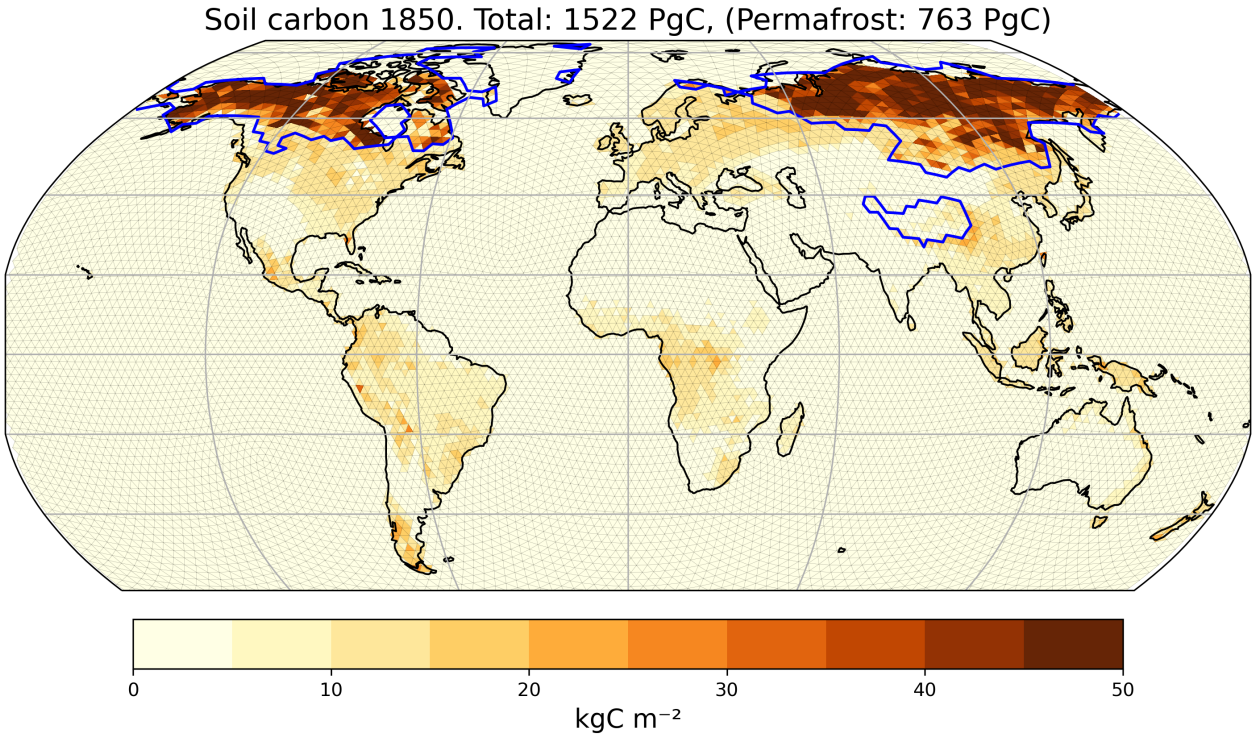

Figure 2. Preindustrial soil carbon distribution $\left[\mathrm{kgC\,m^{-2}}\right]$ after initialisation with Hugelius et al. (2014) permafrost C stock estimate. Outline of permafrost region shown in blue.

permafrost region, of which $434\,\mathrm{PgC}$ are located in permanently frozen soil layers below the active layer, while $328\,\mathrm{PgC}$ are stored within soil layers within the active layer and thus not permanently frozen. Total global preindustrial soil C storage is $1522\,\mathrm{PgC}$ (Figure 2).

Evaluating the carbon stock in comparison to NCSCD further until the present, the active layer deepens during the 20th century due to global warming, as a result of which $340\,\mathrm{PgC}$ remain in frozen soil layers during the 2020s, while $419\,\mathrm{PgC}$ are located in the unfrozen active layer. Meanwhile, the total carbon in the permafrost region stays roughly constant at $759\,\mathrm{PgC}$. As the initialisation data set (Hugelius et al., 2014) showed a total carbon amount of $991\,\mathrm{PgC}$ in the model-determined permafrost zone, the model shows smaller carbon amounts than the observations. Here, two factors could be relevant: first, the model likely misrepresents the active layer thickness, and second, the model is unable to correctly model organic soils. The NCSCD shows that the highest carbon densities are reached in locations with organic soils, and thus the inability to represent organic soils well would lead to a significant underestimate of active layer carbon stocks. At this time it is not possible to decide, which of these two factors is most important.

Expanding the validation of soil carbon storage to global scales, zonal mean carbon storage in ICON-Land compares quite well to observations. In comparison to the WISE30sec data set of soil properties and soil carbon (Batjes, 2016), zonal mean

https://doi.org/10.5194/egusphere-2026-3098
Preprint. Discussion started: 23 June 2026

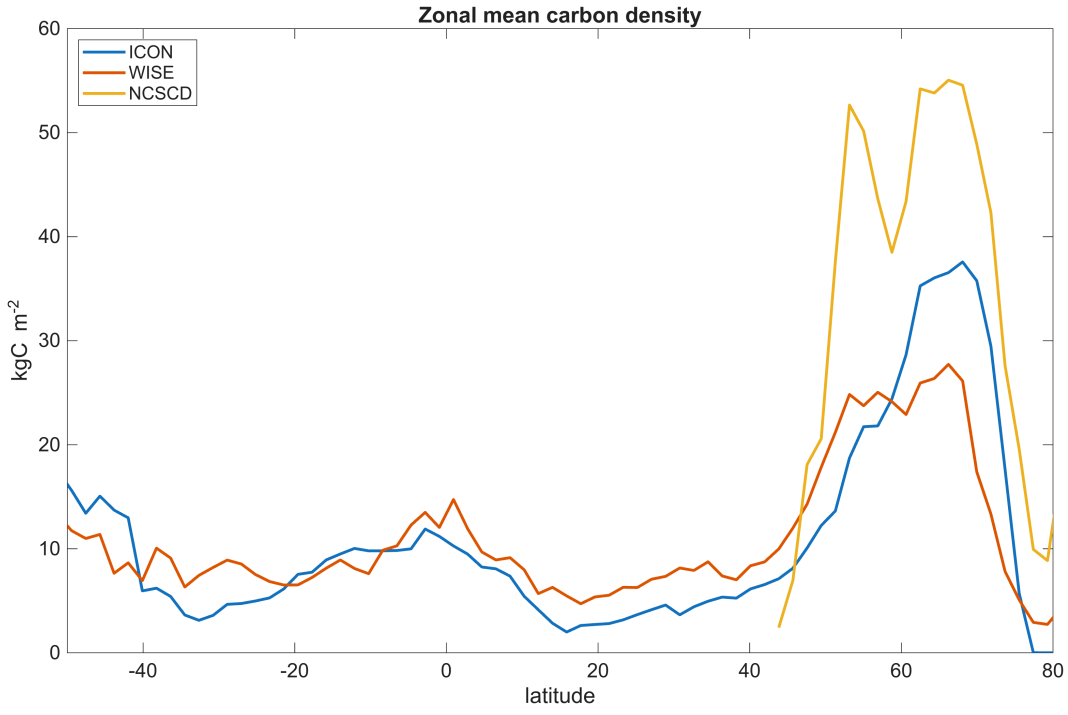

Figure 3. Zonal mean carbon density in ICON-Land, WISE30sec and NCSCDv2.

carbon density in ICON-Land is very comparable in all latitudes below 55°N (Figure 3). Above 55°N, ICON-Land estimates higher carbon densities than WISE30sec, but lower C densities than the NCSCDv2. The discrepancy between these two data sets is largely due to the fact that WISE30sec only estimates C in the upper two metres, while the NCSCDv2 covers the upper three metres of the soil column. The discrepancies between ICON-Land and the NCSCDv2 have a number of causes. First of all, the NCSCDv2 estimates soil carbon in the entire permafrost region, while our model estimate only covers the region of continuous permafrost, as other areas (i.e., discontinuous, sporadic and isolated permafrost) cannot be determined from land surface models at relatively low resolution. Thus, the permafrost region in the NCSCDv2 reaches further south than in our model. Then, our model cannot take organic soils into account fully. The model considers these to be mineral soils, with hydrology largely independent of carbon content, leading to increased drainage and decreased carbon accumulation. As a consequence, carbon storage is underestimated. Finally, there likely are differences in active layer thickness between our model and the locations where C was measured for the NCSCD. As a result, our simulated carbon storage should be expected to be a conservative lower bound estimate.

https://doi.org/10.5194/egusphere-2026-3098
Preprint. Discussion started: 23 June 2026

Table 2. Permafrost region biomass (vegetation) and soil carbon stocks in 2299 CE in all scenario experiments. Initial (2020) values are 53 PgC for biomass, 759 PgC for soil carbon, and 340 PgC for frozen soil carbon stocks. Total carbon in 2020 was 810 PgC.

Experiment	biomass [PgC]	soil [PgC]	frozen [PgC]	total [PgC]
con26	63	719	300	782
con45	75	619	147	694
con85	82	380	0	461
fix26	59	713	299	772
fix45	84	642	145	725
fix85	121	436	0	557
dyn26	68	740	304	807
dyn45	110	698	153	808
dyn85	199	543	0	742

3.3 Permafrost region carbon and vegetation changes

3.3.1 Neglecting CO_2 change

As climate warms during the 21st, 22nd and 23rd centuries, permafrost region soils lose substantial amounts of carbon, as one would expect due to permafrost thaw (Figure 4a). At the beginning of the scenario period in 2020 CE, soil carbon stocks in the permafrost region are 759 PgC, 340 PgC of which are in frozen soil layers. Over the course of the experiment, we see losses of soil carbon commensurate with warming.

These losses are highest in the con85 experiment with constant 2020 CO_2 for photosynthesis and fixed vegetation distribution, while climate follows the high warming RCP 8.5 scenario. Of the 759 PgC stored in soils in 2020, half is lost by 2299, with only 380 PgC remaining in 2299 CE, none of which is in frozen state (Table 2). At the same time, biomass increases moderately from 53 to 82 PgC (+50%), as warmer climatic conditions, especially the longer growing season, lead to more productivity (Figure 4b). As a result, the change in total permafrost region carbon is largest in con85, with total C decreasing from 810 PgC to 461 PgC (-43%, Figure 4c), implying that 349 PgC are released to the atmosphere, thus increasing atmospheric carbon dioxide. As total climate change is reduced in the experiments following the RCP 4.5 and RCP 2.6 scenarios, the carbon cycle changes also become smaller, with con45 releasing 116 PgC to the atmosphere, and con26 releasing 28 PgC.

3.3.2 Neglecting vegetation distribution change

While the permafrost region C cycle changes in the constant CO_2 experiments are largest, they are also least realistic, as it is well known that carbon assimilation in photosynthesis increases with rising atmospheric CO_2. We cover this factor in the 'fix' series of experiments, where photosynthesis is exposed to the CO_2 concentrations from the RCP scenarios 2.6, 4.5, and 8.5, although vegetation distribution is fixed to the 2019 value. In fix85 we see (Figure 4a) that soil carbon decreases by 374 PgC

https://doi.org/10.5194/egusphere-2026-3098
Preprint. Discussion started: 23 June 2026

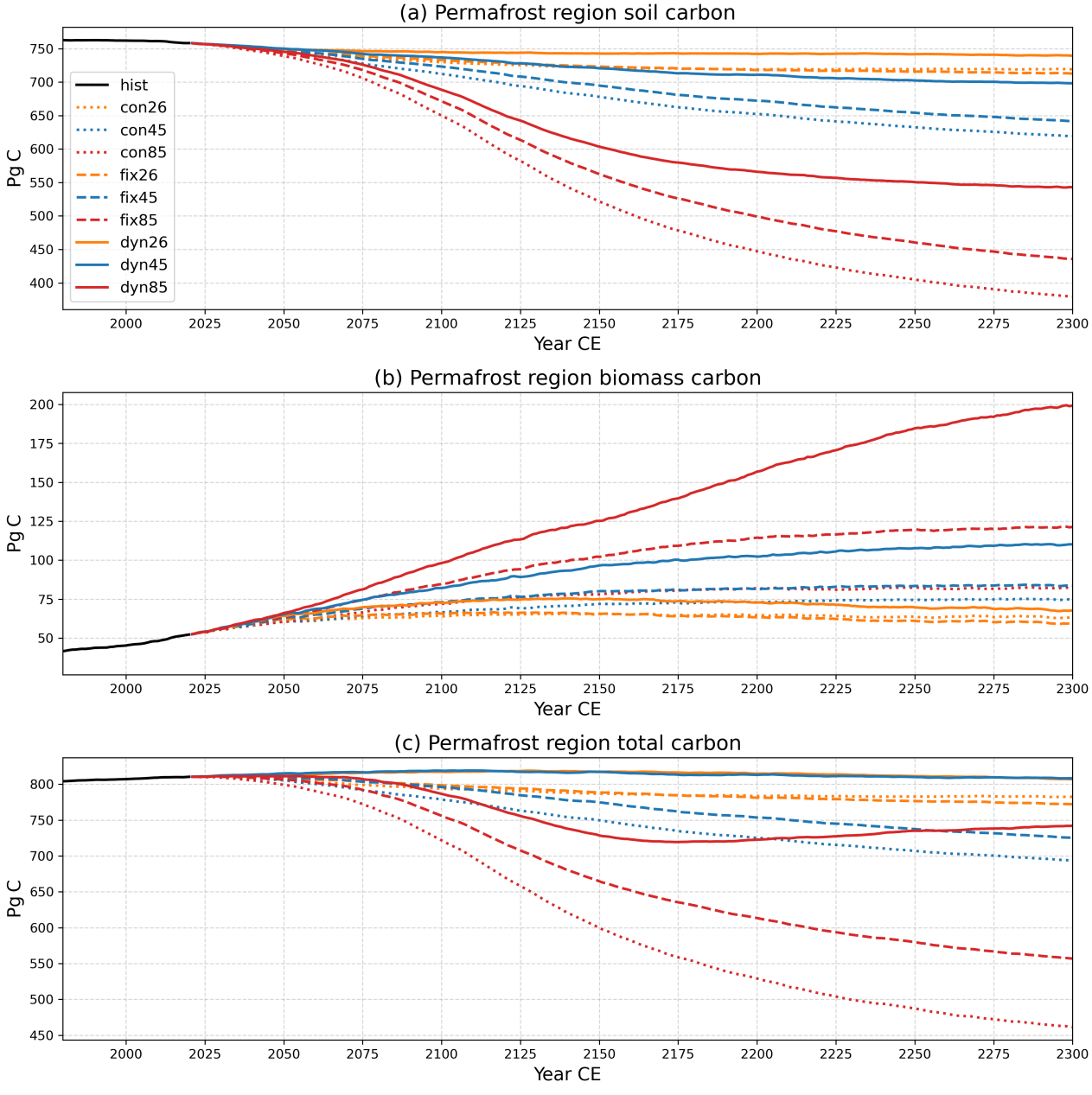

Figure 4. Permafrost region soil (a), biomass (b) and total (c) carbon in historical and scenario experiments, years 1960 to 2300. Dotted lines ('con') assume fixed vegetation and constant 2019 CO_2, while dashed lines ('fix') assume a fixed vegetation distribution after 2019 CE, i.e., no land cover change. Solid lines assume that the vegetation distribution adapts to climate.

https://doi.org/10.5194/egusphere-2026-3098
Preprint. Discussion started: 23 June 2026

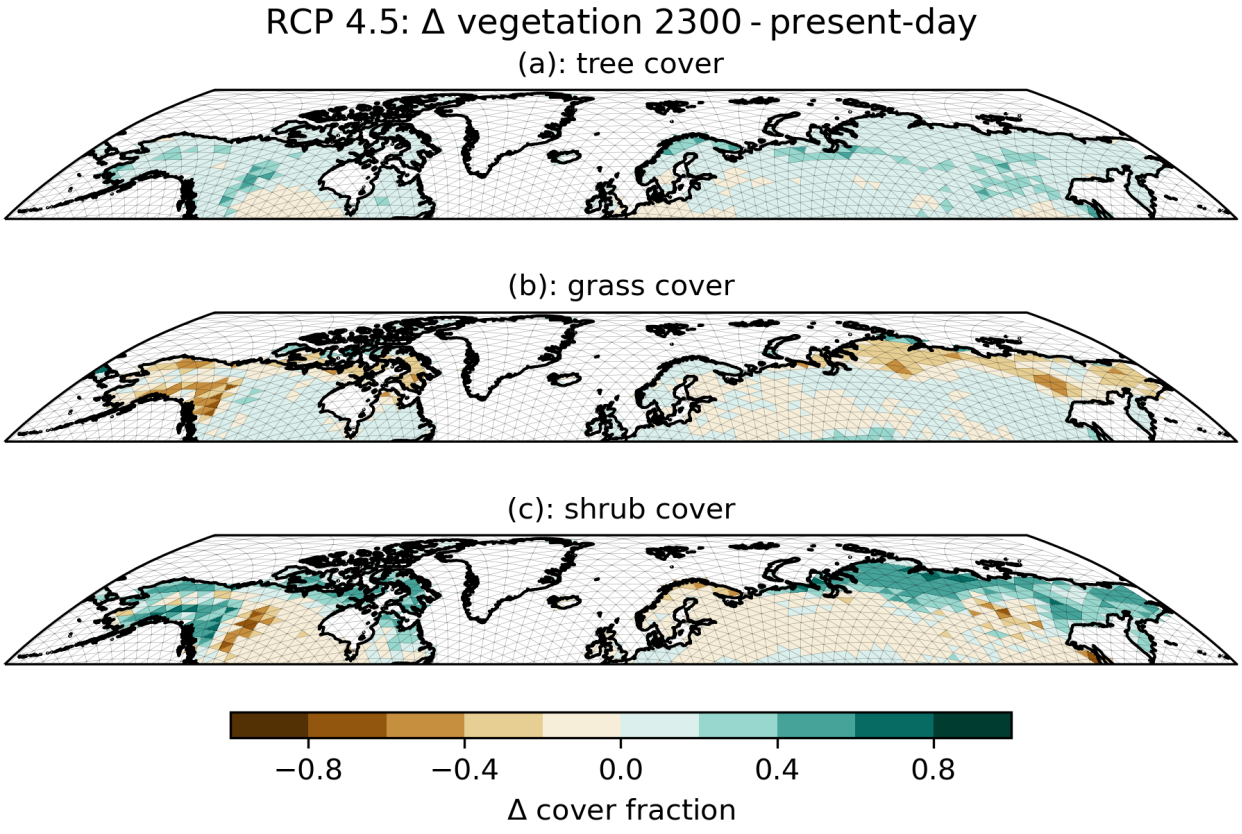

Figure 5. Vegetation cover fraction change in RCP 4.5 between the year 2300 CE and the present for (a) tree cover, (b) grass cover, and (c) shrub cover.

to 436 PgC in 2299 under the RCP 8.5 scenario. At the same time, the increase in biomass is substantially larger than in the con85 experiment, reaching 121 PgC in 2299 CE (+130%, Figure 4b), thus showing a change in total permafrost region C from 810 PgC to 557 PgC (-31%), releasing 253 PgC to the atmosphere. The larger soil C value in 2299 CE is mainly due to the larger biomass production, leading to enhanced litterfall and thus soil carbon formation. In the lower climate change scenarios RCP 4.5 and 2.6, the biomass increase is correspondingly smaller, reaching a change by 38 PgC and 6 PgC in 2299, respectively.

3.3.3 Permafrost region vegetation distribution change

In the final series of experiments, the 'dyn' series, photosynthesis is exposed to the CO_2 concentrations from the RCP scenarios 2.6, 4.5, and 8.5, and modelled vegetation adjusts dynamically to the changes in climate.

There is significant evidence for recent climate change leading to shrubification, and a shift in the northern tree line is less well supported, but expected. Similar to the observational evidence, our experiments show an expansion of shrub cover in

https://doi.org/10.5194/egusphere-2026-3098
Preprint. Discussion started: 23 June 2026

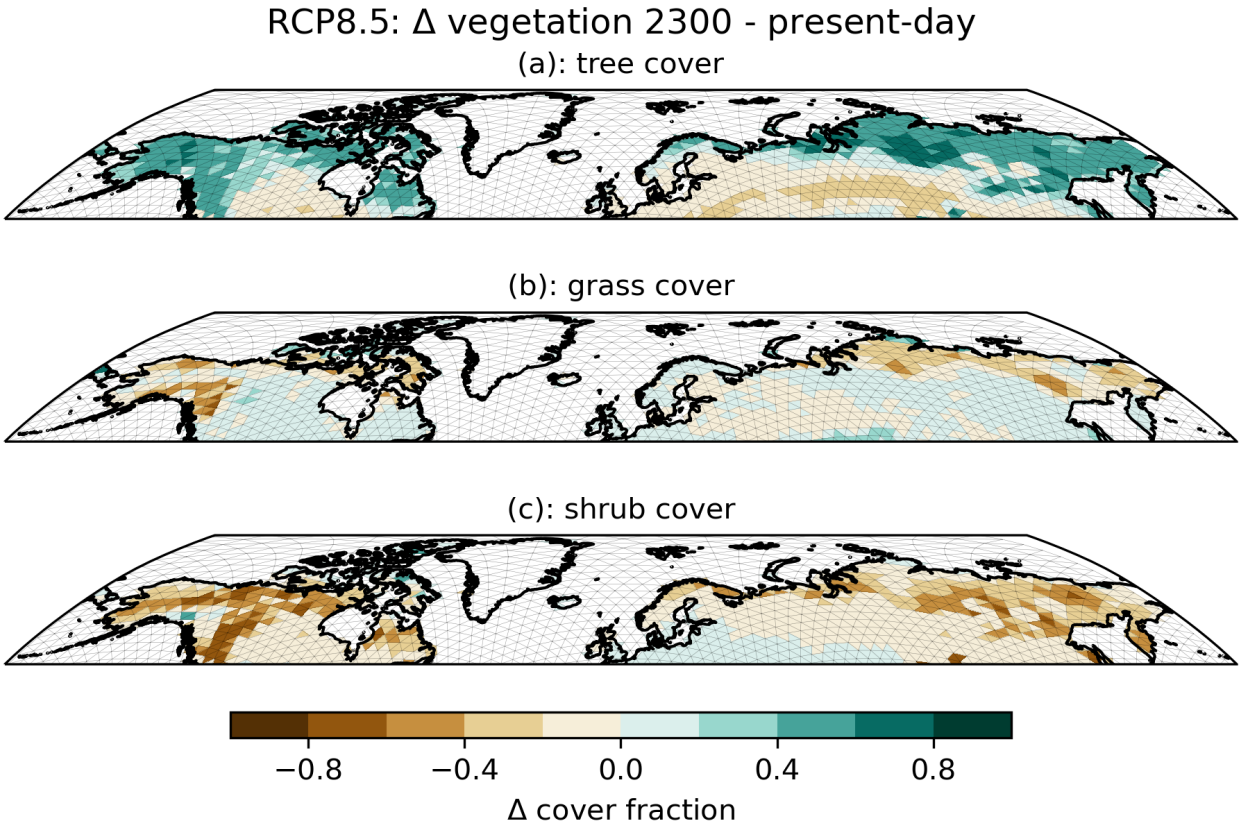

Figure 6. Vegetation cover fraction change in RCP 8.5 between the year 2300 CE and the present for (a) tree cover, (b) grass cover, and (c) shrub cover.

Alaska, the Canadian Arctic, and Siberia under RCP 4.5 (Figure 5). There also is a small increase in tree cover increases in these areas, but at a far smaller magnitude than the change in shrub cover. At the same time, grass cover decreases in those places where shrubs (and trees) expand. Changes in RCP 2.6 (not shown) are qualitatively similar to RCP 4.5, but much smaller in magnitude. Under the stronger warming in RCP 8.5, however, the changes are significantly different. Here, tree cover in Alaska, northern Canada and Siberia expands strongly, at the expense of shrub and, to a smaller extent, grass cover (Figure 6).

3.3.4 Permafrost region carbon cycle changes with vegetation changes

The consequences of the change in vegetation distribution for the carbon cycle are profound. As tree cover increases in experiment dyn85, biomass increases much more strongly than in fix85. While biomass reaches 121 PgC in fix 85, the final value in dyn85 is 199 PgC (+275%). The soil C is also influenced by the vegetation change, as the increase in biomass leads to an additional increase in litterfall. Thus, the decrease in soil is limited to only 216 PgC, substantially less than in fix85 and con85. As

https://doi.org/10.5194/egusphere-2026-3098
Preprint. Discussion started: 23 June 2026

a result, the change in total permafrost region C is qualitatively different in dyn85 than in the other experiments: Here, total C only decreases until 2174 CE, when it reaches a minimum value of $719\,\mathrm{PgC}$. Subsequently, total permafrost region C increases again, until a final value of $742\,\mathrm{PgC}$ (-8%) is reached in 2299 CE. Thus, total C release to the atmosphere under RCP 8.5 is only $68\,\mathrm{PgC}$, substantially less than the $379\,\mathrm{PgC}$ released under the assumptions of constant CO_2 and fixed vegetation. Under scenarios RCP 2.6 and 4.5, total permafrost region C even increases after 2020 CE, reaching a maximum of $819\,\mathrm{PgC}$ in the early 22nd century and decreasing subsequently until a final value of $808\,\mathrm{PgC}$ is reached in 2299 CE, thus showing a carbon release to the atmosphere of only $2\,\mathrm{PgC}$.

4 Discussion

The set of experiments we present in this paper demonstrates that the net carbon balance, and thus the influence on atmospheric CO_2, of the high latitude permafrost region is highly sensitive to the representation of vegetation dynamics and CO_2 fertilisation. When climate warming alone is considered to act on a static vegetation cover, as in the 'con' experiments, permafrost soils lose up to half their original carbon content by 2300 CE, turning the region from a small carbon sink to a significant source, i.e., releasing $\sim 350\,\mathrm{PgC}$ under RCP 8.5 (Figure 4c). If, on the other hand, the model is allowed to adjust vegetation in response to rising CO_2 and climate, as in the 'dyn' experiments, the same climate forcing leads to a significantly smaller net loss of carbon under strong warming (RCP 8.5, $\sim 70\,\mathrm{PgC}$), and potentially even a small gain under low-emission scenarios (RCPs 2.6 and 4.5). these contrasting outcomes highlight the importance of three inter-related mechanisms that act together and can potentially reverse the sign of the permafrost carbon feedback: (i) enhanced NPP and litter input under elevated CO_2, (ii) the expansion of woody PFTs that increase both aboveground biomass and belowground carbon inputs, and (iii) the vertical redistribution of carbon through cryoturbation and bioturbation that is modulated by the changing active-layer thickness.

4.1 CO_2 fertilisation and the 'vegetation-mediated' carbon sink

The 'fix' experiments isolate the effect of rising atmospheric CO_2, while keeping the vegetation distribution frozen in its 2019 state. The resulting increase in biomass (up to $121\,\mathrm{PgC}$ in 'fix85') and reduction in soil-carbon loss relative to the 'con' runs are consistent with studies that have identified CO_2 fertilisation as a major counter-balance to permafrost carbon release (e.g., Schuur et al. (2022)). In our model, the CO_2 effect operates primarily through the Farquhar et al. (1980) model of photosynthesis, which raises leaf-level assimilation rates and translates into higher NPP for all PFTs. The magnitude of the biomass response ($\approx$30% increase under RCP 8.5) is plausible considering the enhancement reported in FACE experiments (e.g., Ainsworth and Long (2005)) and the strong greening inferred from remote sensing (Frost et al., 2025).

Nevertheless, CO_2 fertilisation is subject to uncertainty that may limit its long-term effect. Nutrient limitation, in particular nitrogen limitation, can constrain the additional growth possible due to the higher photosynthetic capacity (Reich et al., 2006). Our current implementation of JSBACH4 does not include an explicit nitrogen cycle, and therefore may overestimate the CO_2 response in nitrogen-poor tundra soils (Schuur et al., 2022). Incorporating a dynamic, nutrient-limited photosynthesis scheme would therefore be a priority for future model development.

https://doi.org/10.5194/egusphere-2026-3098
Preprint. Discussion started: 23 June 2026

4.2 Shrubification, tree expansion and functional-type competition

The 'dyn' experiments allow the vegetation module to respond to climate change, resulting in a pronounced shift from graminoid-dominated tundra toward shrub and, under the strongest warming, tree dominance (Figures 5 and 6). In the observational literature (Sturm et al., 2001; Tape et al., 2006; Myers-Smith et al., 2011) shrubification has been linked to a suite of biophysical feedbacks, including reduced surface albedo, altered snow insulation, and increased evapotranspiration (Kaplan et al., 2003; Schuur et al., 2022). Our model reproduces the spatial pattern of shrub coverage reported by the high-resolution Sentinel-based land-cover product of Bartsch et al. (2024a), albeit with a slightly larger magnitude in western Canada. The addition of a cold-tolerant shrub PFT, parameterised following Kaplan et al. (2003), is essential for capturing this response; without it, the DYNVEG scheme would unrealistically favour grasses in the coldest parts of the domain (see Section 3.1).

The most striking outcome of the 'dyn' runs is the near-cancellation of soil-carbon loss by the increase in woody biomass under RCP 8.5. Tree cover expands dramatically in Alaska, northern Canada and Siberia, raising total aboveground carbon from $53\,\mathrm{PgC}$ (2020) to $199\,\mathrm{PgC}$ (2299). The model's competition algorithm, which favours PFTs with higher NPP, naturally leads to a rapid takeover of newly suitable habitats by shrubs and trees once the growing-season length exceeds the GDD threshold. This mechanistic representation aligns with the palaeo-ecological evidence for northward tree migration during the early Holocene (Bigelow et al., 2003; Williams, 2003), and recent remote-sensing evidence seems to support a northward shift of boreal tree cover (Feng et al., 2026), despite earlier estimates not confirming this for North America (Rotbarth et al., 2023).

However, the representation of disturbance (fire, windthrow) in our model is highly simplified; increased fire frequency under warming could significantly affect shrub and tree cover expansion by removing biomass and exposing soil organic matter (Liu et al., 2022; Burrell et al., 2022).

4.3 Model–data comparison and sources of bias

Our pre-industrial soil-carbon inventory (Figure 2) reproduces the broad spatial pattern of the Northern Circumpolar Soil Carbon Database (NCSCDv2; Hugelius et al. (2014)) but underestimates the total stock ($763\,\mathrm{PgC}$ vs. $991\,\mathrm{PgC}$ (taking the model-determined permafrost domain) or even $1035\,\mathrm{PgC}$ (taking the Hugelius et al. (2014) permafrost domain)). Three non-exclusive explanations are plausible. First, the model's inability to properly represent organic soils with their tighter coupling of carbon cycle and hydrology leads to an underestimation of carbon in peatlands, which dominate the active-layer carbon pool. Second, we might underestimate the carbon allocated to the humus pool, thus overestimating decomposability of the SOM. Third, the active-layer thickness in the model is likely different from what might be observable in the field, affecting the amount of carbon that can be stored.

The vegetation validation (Figure 1) shows a systematic underestimation of larch-dominated tree cover in Siberia, reflecting the inability of the present dynamical vegetation scheme to account for tree cover in this ecosystem. This bias likely contributes to the lower simulated NPP in those regions, and consequently to a reduced litter input to the soil. Adding a larch PFT with appropriate phenology and cold tolerance might improve the representation of boreal forest dynamics and could increase the modelled carbon sink under the 'dyn' experiments.

https://doi.org/10.5194/egusphere-2026-3098
Preprint. Discussion started: 23 June 2026

5 Conclusions

Our model experiments demonstrate the profound influence of vegetation dynamics on the permafrost region carbon balance. When strong climate warming is applied to permafrost soils with a static vegetation cover (the 'con' experiments), permafrost soils lose roughly half of their carbon stock by the end of the 23rd century, turning the high-latitude region from a modest sink into a strong source of carbon ($\approx 350\,\mathrm{PgC}$ released under RCP 8.5; Figure 4c). Allowing the vegetation to respond to both the rising CO_2 and warming (the 'dyn' experiments) dramatically reduces this loss ($\approx 70\,\mathrm{PgC}$ under the same forcing) and yields no change to potentially even a small net gain under low-emission pathways (RCP 2.6 and 4.5). These contrasting outcomes demonstrate that the sign and magnitude of the permafrost carbon feedback are highly contingent on the representation of plant functional type (PFT) competition, CO_2 fertilisation, and the resulting shifts in NPP and litter input.

Experiments that expose photosynthesis to the RCP-driven CO_2 trajectory while keeping vegetation fixed ('fix' series) increase aboveground biomass by up to $121\,\mathrm{PgC}$ (RCP 8.5) and partially offset soil-carbon losses. While an increase in biomass is consistent with FACE experiments that report enhancements of NPP under elevated CO_2 (Ainsworth and Long, 2005), this strong response to CO_2 fertilisation may be overly optimistic, as the model currently lacks an explicit nitrogen cycle, which may lead to an overestimate of the fertilisation effect in nutrient-limited soils (Reich et al., 2006). Incorporating nutrient limitation will be essential for quantifying the long-term sustainability of this sink.

Shrubification and tree expansion reshape carbon inputs and surface properties. The addition of a cold-resistant shrub PFT enables a realistic simulation of the well-documented Arctic shrubification (Sturm et al., 2001; Myers-Smith et al., 2011). Under moderate warming (RCP 4.5), we see shrubs expanding across Alaska, western Canada and Siberia, while grasses retreat. Under the strongest warming (RCP 8.5) the model predicts a pronounced northward shift of tree cover, with the resulting increase in woody biomass (up to $199\,\mathrm{PgC}$ in dyn85) supplying additional litter, thus limiting soil C loss to only $216\,\mathrm{PgC}$, despite complete thawing of the (former) permafrost soils.

Model–data mismatches point to key opportunities for model improvement. The preindustrial soil carbon inventory ($763\,\mathrm{PgC}$) in the permafrost region underestimates the NCSCDv2 estimate ($\approx 1000\,\mathrm{PgC}$) by ~20%. This shortfall is primarily driven by the neglected consideration of organic soil (largely due to lacking hydrology), which leads to low carbon densities in peat-dominated tundra, and a possible bias in simulated active layer thickness. Likewise, the underestimate of the larch-dominated boreal forests in Siberia suggests the need for improvements to the dynamical vegetation representation. Addressing these structural issues will improve both the baseline carbon pool representation and the model sensitivity to climate-driven vegetation change.

Code and data availability. The primary data, i.e. the model code for ICON-Land, will be part of the ICON model open source release at https://www.icon-model.org by the time peer review of this manuscript is finished. The exact model code used in this publication, as well as configuration files, the model output used in this manuscript, and plotting scripts, is archived in the EDMOND open research data repository and can be accessed at https://doi.org/10.17617/3.1ROAHN (Kleinen et al., 2026).

https://doi.org/10.5194/egusphere-2026-3098
Preprint. Discussion started: 23 June 2026

Author contributions. TK: Model development, experiment design and analysis, main author of text. HB: Shrub data integration, interpretation of results. PdV: Model development, interpretation of results. TS: Model development, interpretation of results. VB: Experiment interpretation. All: Discussion of results, editing of manuscript.

Competing interests. The authors declare that there are no competing interests.

Acknowledgements. We thank Mateo Duque Villegas for his comments on an earlier version of this manuscript.

Thomas Kleinen, Helena Bergstedt, Philipp de Vrese, Tobias Stacke, and Victor Brovkin acknowledge funding by the European Research Council under the European Union's Horizon 2020 Research and Innovation programme as part of the Q-Arctic project (Grant 951288). Thomas Kleinen also acknowledges funding by the Deutsche Forschungsgemeinschaft (DFG, German Research Foundation) under Germany's Excellence Strategy – EXC 2037 'CLICCS - Climate, Climatic Change, and Society' – Project Number: 390683824.

This work used resources of the Deutsches Klimarechenzentrum (DKRZ) granted by its Scientific Steering Committee (WLA) for Q-Arctic (under project ID bm1236).

In the preparation of this manuscript, we made use of AI: We used AI for literature search, as well as for debugging plotting scripts. Finally, we used AI to provide initial drafts for both the introduction and discussion sections. These sections were subsequently edited extensively.

https://doi.org/10.5194/egusphere-2026-3098
Preprint. Discussion started: 23 June 2026

References

Ainsworth, E. A. and Long, S. P.: What have we learned from 15 years of free-air CO_2 enrichment (FACE)? A meta-analytic review of the responses of photosynthesis, canopy properties and plant production to rising CO_2, New Phytologist, 165, 351–372, https://doi.org/10.1111/j.1469-8137.2004.01224.x, 2005.

Bartsch, A., Efimova, A., Widhalm, B., Muri, X., von Baeckmann, C., Bergstedt, H., Ermokhina, K., Hugelius, G., Heim, B., and Leibman, M.: Circumarctic land cover diversity considering wetness gradients, Hydrology and Earth System Sciences, 28, 2421–2481, https://doi.org/10.5194/hess-28-2421-2024, 2024a.

Bartsch, A., Khairullin, R., Efimova, A., Widhalm, B., Muri, X., von Baeckmann, C., Bergstedt, H., Ermokhina, K., Hugelius, G., Heim, B., Leibman, M., and Gruber, C.: Circumarctic Landcover Units [data set], https://doi.org/10.5281/zenodo.14235736, 2024b.

Batjes, N.: Harmonized soil property values for broad-scale modelling (WISE30sec) with estimates of global soil carbon stocks, Geoderma, 269, 61–68, https://doi.org/10.1016/j.geoderma.2016.01.034, 2016.

Bigelow, N. H., Brubaker, L. B., Edwards, M. E., Harrison, S. P., Prentice, I. C., Anderson, P. M., Andreev, A. A., Bartlein, P. J., Christensen, T. R., Cramer, W., Kaplan, J. O., Lozhkin, A. V., Matveyeva, N. V., Murray, D. F., McGuire, A. D., Razzhivin, V. Y., Ritchie, J. C., Smith, B., Walker, D. A., Gajewski, K., Wolf, V., Holmqvist, B. H., Igarashi, Y., Kremenetskii, K., Paus, A., Pisaric, M. F. J., and Volkova, V. S.: Climate change and Arctic ecosystems: 1. Vegetation changes north of 55 degrees N between the last glacial maximum, mid-Holocene, and present, Journal of Geophysical Research, D19, 8170, https://doi.org/10.1029/2002JD002558, 2003.

Brovkin, V., Raddatz, T., Reick, C. H., Claussen, M., and Gayler, V.: Global biogeophysical interactions between forest and climate, Geophysical Research Letters, 36, L07 702, https://doi.org/10.1029/2008GL036759, 2009.

Brovkin, V., Boysen, L., Raddatz, T., Gayler, V., Loew, A., and Claussen, M.: Evaluation of vegetation cover and land-surface albedo in MPI-ESM CMIP5 simulations, Journal of Advances in Modeling Earth Systems, 5, 48–57, https://doi.org/10.1029/2012MS000169, 2013.

Burke, E. J., Chadburn, S. E., and Ekici, A.: A vertical representation of soil carbon in the JULES land surface scheme (vn4.3_permafrost) with a focus on permafrost regions, Geoscientific Model Development, 10, 959–975, https://doi.org/10.5194/gmd-10-959-2017, 2017a.

Burke, E. J., Ekici, A., Huang, Y., Chadburn, S. E., Huntingford, C., Ciais, P., Friedlingstein, P., Peng, S., and Krinner, G.: Quantifying uncertainties of permafrost carbon–climate feedbacks, Biogeosciences, 14, 3051–3066, https://doi.org/10.5194/bg-14-3051-2017, 2017b.

Burrell, A. L., Sun, Q., Baxter, R., Kukavskaya, E. A., Zhila, S., Shestakova, T., Rogers, B. M., Kaduk, J., and Barrett, K.: Climate change, fire return intervals and the growing risk of permanent forest loss in boreal Eurasia, Science of The Total Environment, 831, 154 885, https://doi.org/10.1016/j.scitotenv.2022.154885, 2022.

C3S CDS, C.: Land cover classification gridded maps from 1992 to present derived from satellite observation [data set], https://doi.org/10.24381/cds.006f2c9a, 2019.

Chojnacky, D., Amacher, M., and Gavazzi, M.: Separating Duff and Litter for Improved Mass and Carbon Estimates, Southern Journal of Applied Forestry, 33, 29–34, https://doi.org/10.1093/sjaf/33.1.29, 2009.

Dallmeyer, A., Claussen, M., Lorenz, S. J., Sigl, M., Toohey, M., and Herzschuh, U.: Holocene vegetation transitions and their climatic drivers in MPI-ESM1.2, Climate of the Past, 17, 2481–2513, https://doi.org/10.5194/cp-17-2481-2021, 2021.

Dallmeyer, A., Poska, A., Marquer, L., Seim, A., and Gaillard, M.-J.: The challenge of comparing pollen-based quantitative vegetation reconstructions with outputs from vegetation models – a European perspective, Climate of the Past, 19, 1531–1557, https://doi.org/10.5194/cp-19-1531-2023, 2023.

https://doi.org/10.5194/egusphere-2026-3098
Preprint. Discussion started: 23 June 2026

de Vrese, P., Stacke, T., Kleinen, T., and Brovkin, V.: Diverging responses of high-latitude CO_2 and CH_4 emissions in idealized climate change scenarios, The Cryosphere, 15, 1097–1130, https://doi.org/10.5194/tc-15-1097-2021, 2021.

Defourny, P., Lamarche, C., Bontemps, S., De Maet, T., Van Bogaert, E., Moreau, I., Brockmann, C., Boettcher, M., Kirches, G., Wevers, J., Santoro, M., Ramoino, F., and Arino, O.: Land Cover Climate Change Initiative - Product User Guide v2, Tech. rep., http://maps.elie.ucl.ac.be/CCI/viewer/download/ESACCI-LC-Ph2-PUGv2_2.0.pdf, 2017.

FAO: Digital Soil Map of the World, DSMW, https://fao.org, 2003.

Farquhar, G. D., von Caemmerer, S., and Berry, J. A.: A biochemical model of photosynthetic CO_2 assimilation in leaves of C3 species, Planta, 149, 78–90, https://doi.org/10.1007/BF00386231, 1980.

Feng, M., Sexton, J. O., Wang, P., Montesano, P. M., Calle, L., Carvalhais, N., Poulter, B., Macander, M. J., Wulder, M. A., Wooten, M., Wagner, W., Elders, A., Channan, S., and Neigh, C. S. R.: Northward shift of boreal tree cover confirmed by satellite record, Biogeosciences, 23, 1089–1101, https://doi.org/10.5194/bg-23-1089-2026, 2026.

Frost, G. V., Bhatt, U. S., Macander, M. J., Berner, L. T., Walker, D. A., Raynolds, M. K., Magnússon, R. I., Bartsch, A., Bjerke, J. W., Epstein, H. E., Forbes, B. C., Goetz, S. J., Hoy, E. E., Karlsen, S. R., Kumpula, T., Lantz, T. C., Lara, M. J., López-Blanco, E., Montesano, P. M., Neigh, C. S. R., Nitze, I., Orndahl, K. M., Park, T., Phoenix, G. K., Rocha, A. V., Rogers, B. M., Schaepman-Strub, G., Tømmervik, H., Verdonen, M., Veremeeva, A., Virkkala, A.-M., and Waigl, C. F.: The changing face of the Arctic: four decades of greening and implications for tundra ecosystems, Frontiers in Environmental Science, 13, https://doi.org/10.3389/fenvs.2025.1525574, 2025.

García-Pereira, F., González-Rouco, J. F., Meabe-Yanguas, N., de Vrese, P., Steinert, N. J., Jungclaus, J., and Lorenz, S.: Permafrost sensitivity to soil hydro-thermodynamics in historical and scenario simulations with the MPI-ESM, The Cryosphere, 19, 5959–5981, https://doi.org/10.5194/tc-19-5959-2025, 2025.

Giorgetta, M. A., Jungclaus, J., Reick, C. H., Legutke, S., Bader, J., Böttinger, M., Brovkin, V., Crueger, T., Esch, M., Fieg, K., Glushak, K., Gayler, V., Haak, H., Hollweg, H.-D., Ilyina, T., Kinne, S., Kornblueh, L., Matei, D., Mauritsen, T., Mikolajewicz, U., Mueller, W., Notz, D., Pithan, F., Raddatz, T., Rast, S., Redler, R., Roeckner, E., Schmidt, H., Schnur, R., Segschneider, J., Six, K. D., Stockhause, M., Timmreck, C., Wegner, J., Widmann, H., Wieners, K.-H., Claussen, M., Marotzke, J., and Stevens, B.: Climate and carbon cycle changes from 1850 to 2100 in MPI-ESM simulations for the Coupled Model Intercomparison Project phase 5, Journal of Advances in Modeling Earth Systems, 5, 572–597, https://doi.org/10.1002/jame.20038, 2013.

Goll, D. S., Brovkin, V., Liski, J., Raddatz, T., Thum, T., and Todd-Brown, K. E. O.: Strong dependence of CO_2 emissions from anthropogenic land cover change on initial land cover and soil carbon parametrization, Global Biogeochemical Cycles, 29, 1511–1523, https://doi.org/10.1002/2014GB004988, 2015.

Hagemann, S. and Stacke, T.: Impact of the soil hydrology scheme on simulated soil moisture memory, Climate Dynamics, 44, 1731–1750, https://doi.org/10.1007/s00382-014-2221-6, 2015.

Harper, K. L., Lamarche, C., Hartley, A., Peylin, P., Ottlé, C., Bastrikov, V., San Martín, R., Bohnenstengel, S. I., Kirches, G., Boettcher, M., Shevchuk, R., Brockmann, C., and Defourny, P.: A 29-year time series of annual 300 m resolution plant-functional-type maps for climate models, Earth System Science Data, 15, 1465–1499, https://doi.org/10.5194/essd-15-1465-2023, 2023.

Hugelius, G., Strauss, J., Zubrzycki, S., Harden, J. W., Schuur, E. A. G., Ping, C.-L., Schirrmeister, L., Grosse, G., Michaelson, G. J., Koven, C. D., O'Donnell, J. A., Elberling, B., Mishra, U., Camill, P., Yu, Z., Palmtag, J., and Kuhry, P.: Estimated stocks of circumpolar permafrost carbon with quantified uncertainty ranges and identified data gaps, Biogeosciences, 11, 6573–6593, https://doi.org/10.5194/bg-11-6573-2014, 2014.

https://doi.org/10.5194/egusphere-2026-3098
Preprint. Discussion started: 23 June 2026

Jackson, R. B., Canadell, J., Ehleringer, J. R., Mooney, H. A., Sala, O. E., and Schulze, E. D.: A global analysis of root distributions for terrestrial biomes, Oecologia, 108, 389–411, https://doi.org/10.1007/BF00333714, 1996.

Kaplan, J. O., Bigelow, N. H., Prentice, I. C., Harrison, S. P., Bartlein, P. J., Christensen, T. R., Cramer, W., Matveyeva, N. V., McGuire, A. D., Murray, D. F., Razzhivin, V. Y., Smith, B., Walker, D. A., Anderson, P. M., Andreev, A. A., Brubaker, L. B., Edwards, M. E., and Lozhkin, A. V.: Climate change and Arctic ecosystems: 2. Modeling, paleodata-model comparisons, and future projections, Journal of Geophysical Research: Atmospheres, 108, https://doi.org/10.1029/2002JD002559, 2003.

Kelly, R. H., Parton, W. J., Hartman, M. D., Stretch, L. K., Ojima, D. S., and Schimel, D. S.: Intra-annual and interannual variability of ecosystem processes in shortgrass steppe, Journal of Geophysical Research: Atmospheres, 105, 20 093–20 100, https://doi.org/10.1029/2000JD900259, 2000.

Kleinen, T. and Brovkin, V.: Pathway-dependent fate of permafrost region carbon, Environmental Research Letters, 13, 094 001, https://doi.org/10.1088/1748-9326/aad824, 2018.

Kleinen, T., Bergstedt, H., de Vrese, P., Stacke, T., and Brovkin, V.: Reassessing the Permafrost Carbon Feedback: The Decisive Role of Dynamic Vegetation [Data set], https://doi.org/10.17617/3.1ROAHN, 2026.

Koven, C. D., Ringeval, B., Friedlingstein, P., Ciais, P., Cadule, P., Khvorostyanov, D., Krinner, G., and Tarnocai, C.: Permafrost carbon-climate feedbacks accelerate global warming, Proceedings of the National Academy of Sciences, 108, 14 769–14 774, https://doi.org/10.1073/pnas.1103910108, 2011.

Koven, C. D., Lawrence, D. M., and Riley, W. J.: Permafrost carbon-climate feedback is sensitive to deep soil carbon decomposability but not deep soil nitrogen dynamics, Proceedings of the National Academy of Sciences, 112, 3752–3757, https://doi.org/10.1073/pnas.1415123112, 2015.

Li, C., Dallmeyer, A., Ni, J., Chevalier, M., Willeit, M., Andreev, A. A., Cao, X., Schild, L., Heim, B., Wieczorek, M., and Herzschuh, U.: Global biome changes over the last 21 000 years inferred from model–data comparisons, Climate of the Past, 21, 1001–1024, https://doi.org/10.5194/cp-21-1001-2025, 2025.

Liski, J., Palosuo, T., Peltoniemi, M., and Sievänen, R.: Carbon and decomposition model Yasso for forest soils, Ecological Modelling, 189, 168–182, https://doi.org/10.1016/j.ecolmodel.2005.03.005, 2005.

Liu, Y., Riley, W. J., Keenan, T. F., Mekonnen, Z. A., Holm, J. A., Zhu, Q., and Torn, M. S.: Dispersal and fire limit Arctic shrub expansion, Nature Communications, 13, 3843, https://doi.org/10.1038/s41467-022-31597-6, 2022.

Mauritsen, T., Bader, J., Becker, T., Behrens, J., Bittner, M., Brokopf, R., Brovkin, V., Claussen, M., Crueger, T., Esch, M., Fast, I., Fiedler, S., Fläschner, D., Gayler, V., Giorgetta, M., Goll, D. S., Haak, H., Hagemann, S., Hedemann, C., Hohenegger, C., Ilyina, T., Jahns, T., Jimenéz-de-la Cuesta, D., Jungclaus, J., Kleinen, T., Kloster, S., Kracher, D., Kinne, S., Kleberg, D., Lasslop, G., Kornblueh, L., Marotzke, J., Matei, D., Meraner, K., Mikolajewicz, U., Modali, K., Möbis, B., Müller, W. A., Nabel, J. E. M. S., Nam, C. C. W., Notz, D., Nyawira, S.-S., Paulsen, H., Peters, K., Pincus, R., Pohlmann, H., Pongratz, J., Popp, M., Raddatz, T. J., Rast, S., Redler, R., Reick, C. H., Rohrschneider, T., Schemann, V., Schmidt, H., Schnur, R., Schulzweida, U., Six, K. D., Stein, L., Stemmler, I., Stevens, B., von Storch, J.-S., Tian, F., Voigt, A., Vrese, P., Wieners, K.-H., Wilkenskjeld, S., Winkler, A., and Roeckner, E.: Developments in the MPI-M Earth System Model version 1.2 (MPI-ESM1.2) and its response to increasing CO_2, Journal of Advances in Modeling Earth Systems, 11, 998–1038, https://doi.org/10.1029/2018MS001400, 2019.

McGuire, A. D., Koven, C., Lawrence, D. M., Clein, J. S., Xia, J., Beer, C., Burke, E., Chen, G., Chen, X., Delire, C., Jafarov, E., MacDougall, A. H., Marchenko, S., Nicolsky, D., Peng, S., Rinke, A., Saito, K., Zhang, W., Alkama, R., Bohn, T. J., Ciais, P., Decharme, B., Ekici, A., Gouttevin, I., Hajima, T., Hayes, D. J., Ji, D., Krinner, G., Lettenmaier, D. P., Luo, Y., Miller, P. A., Moore, J. C., Romanovsky, V.,

https://doi.org/10.5194/egusphere-2026-3098
Preprint. Discussion started: 23 June 2026

Schädel, C., Schaefer, K., Schuur, E. A., Smith, B., Sueyoshi, T., and Zhuang, Q.: Variability in the sensitivity among model simulations of permafrost and carbon dynamics in the permafrost region between 1960 and 2009, Global Biogeochemical Cycles, 30, 1015–1037, https://doi.org/10.1002/2016GB005405, 2016.

Meinshausen, M., Smith, S. J., Calvin, K., Daniel, J. S., Kainuma, M. L. T., Lamarque, J.-F., Matsumoto, K., Montzka, S. A., Raper, S. C. B., Riahi, K., Thomson, A., Velders, G. J. M., and van Vuuren, D. P.: The RCP greenhouse gas concentrations and their extensions from 1765 to 2300, Climatic Change, 109, 213, https://doi.org/10.1007/s10584-011-0156-z, 2011.

Myers-Smith, I. H., Forbes, B. C., Wilmking, M., Hallinger, M., Lantz, T., Blok, D., Tape, K. D., Macias-Fauria, M., Sass-Klaassen, U., Lévesque, E., Boudreau, S., Ropars, P., Hermanutz, L., Trant, A., Collier, L. S., Weijers, S., Rozema, J., Rayback, S. A., Schmidt, N. M., Schaepman-Strub, G., Wipf, S., Rixen, C., Ménard, C. B., Venn, S., Goetz, S., Andreu-Hayles, L., Elmendorf, S., Ravolainen, V., Welker, J., Grogan, P., Epstein, H. E., and Hik, D. S.: Shrub expansion in tundra ecosystems: dynamics, impacts and research priorities, Environmental Research Letters, 6, 045 509, https://doi.org/10.1088/1748-9326/6/4/045509, 2011.

Obu, J.: How Much of the Earth's Surface is Underlain by Permafrost?, Journal of Geophysical Research: Earth Surface, 126, e2021JF006 123, https://doi.org/10.1029/2021JF006123, e2021JF006123 2021JF006123, 2021.

O'Donnell, J. A., Romanovsky, V. E., Harden, J. W., and McGuire, A. D.: The Effect of Moisture Content on the Thermal Conductivity of Moss and Organic Soil Horizons From Black Spruce Ecosystems in Interior Alaska, Soil Science, 174, 2009.

Palmtag, J., Obu, J., Kuhry, P., Richter, A., Siewert, M. B., Weiss, N., Westermann, S., and Hugelius, G.: A high spatial resolution soil carbon and nitrogen dataset for the northern permafrost region based on circumpolar land cover upscaling, Earth System Science Data, 14, 4095–4110, https://doi.org/10.5194/essd-14-4095-2022, 2022.

Rantanen, M., Karpechko, A. Y., Lipponen, A., Nordling, K., Hyvärinen, O., Ruosteenoja, K., Vihma, T., and Laaksonen, A.: The Arctic has warmed nearly four times faster than the globe since 1979, Communications Earth & Environment, p. 168, https://doi.org/10.1038/s43247-022-00498-3, 2022.

Reich, P. B., Hobbie, S. E., Lee, T., Ellsworth, D. S., West, J. B., Tilman, D., Knops, J. M. H., Naeem, S., and Trost, J.: Nitrogen limitation constrains sustainability of ecosystem response to CO_2, Nature, 440, 922–925, https://doi.org/10.1038/nature04486, 2006.

Reick, C. H., Raddatz, T., Brovkin, V., and Gayler, V.: Representation of natural and anthropogenic land cover change in MPI-ESM, Journal of Advances in Modeling Earth Systems, 5, 459–482, https://doi.org/10.1002/jame.20022, 2013.

Reick, C. H., Gayler, V., Goll, D., Hagemann, S., Heidkamp, M., Nabel, J. E., Raddatz, T., Roeckner, E., Schnur, R., and Wilkenskjeld, S.: JSBACH 3 - The land component of the MPI Earth System Model: documentation of version 3.2, Tech. Rep. Berichte zur Erdsystemforschung 240, Max-Planck Institut für Meteorologie, Hamburg, Germany, https://doi.org/10.17617/2.3279802, 2021.

Romanovsky, V., Isaksen, K., Drozdov, D., Anisimov, O., Instanes, A., Leibman, M., McGuire, A. D., Shiklomanov, N., Smith, S., and Walker, D.: Changing permafrost and its impacts, in: Snow, Water, Ice and Permafrost in the Arctic (SWIPA), pp. 65 – 102, Arctic Monitoring and Assessment Programme (AMAP), Oslo, Norway, 2017.

Rotbarth, R., Van Nes, E. H., Scheffer, M., Jepsen, J. U., Vindstad, O. P. L., Xu, C., and Holmgren, M.: Northern expansion is not compensating for southern declines in North American boreal forests, Nature Communications, 14, 3373, https://doi.org/10.1038/s41467-023-39092-2, 2023.

Rotbarth, R., van Nes, E. H., Scheffer, M., and Holmgren, M.: Boreal forests are heading for an open state, Proceedings of the National Academy of Sciences, 122, e2404391 121, https://doi.org/10.1073/pnas.2404391121, 2025.

Schaefer, K., Zhang, T., Bruhwiler, L., and Barrett, A. P.: Amount and timing of permafrost carbon release in response to climate warming, Tellus B, 63, 165–180, https://doi.org/10.1111/j.1600-0889.2011.00527.x, 2011.

https://doi.org/10.5194/egusphere-2026-3098
Preprint. Discussion started: 23 June 2026

Schneck, R., Gayler, V., Nabel, J. E. M. S., Raddatz, T., Reick, C. H., and Schnur, R.: Assessment of JSBACHv4.30 as a land component of ICON-ESM-V1 in comparison to its predecessor JSBACHv3.2 of MPI-ESM1.2, Geoscientific Model Development, 15, 8581–8611, https://doi.org/10.5194/gmd-15-8581-2022, 2022.

Schuur, E. A., Abbott, B. W., Commane, R., Ernakovich, J., Euskirchen, E., Hugelius, G., Grosse, G., Jones, M., Koven, C., Leshyk, V., Lawrence, D., Loranty, M. M., Mauritz, M., Olefeldt, D., Natali, S., Rodenhizer, H., Salmon, V., Schädel, C., Strauss, J., Treat, C., and Turetsky, M.: Permafrost and Climate Change: Carbon Cycle Feedbacks From the Warming Arctic, Annual Review of Environment and Resources, 47, 343–371, https://doi.org/10.1146/annurev-environ-012220-011847, 2022.

Schuur, E. A. G., McGuire, A. D., Schädel, C., Koven, C. D., Lawrence, D. M., Natali, S. M., O'Neill, J. L., Rupp, T. S., Schaefer, K., Swenson, S. C., Turetsky, M. R., Vertenstein, M., and Zimov, S. A.: Climate change and the permafrost carbon feedback, Nature, 520, 171–179, https://doi.org/10.1038/nature14338, 2015.

Sturm, M., Racine, C., and Tape, K.: Increasing shrub abundance in the Arctic, Nature, 411, 546–547, https://doi.org/10.1038/35079180, 2001.

Tape, K., Sturm, M., and Racine, C.: The evidence for shrub expansion in Northern Alaska and the Pan-Arctic, Global Change Biology, 12(5), 686–702, https://doi.org/doi:10.1111/j.1365-2486.2006.01128.x, 2006.

Tuomi, M., Vanhala, P., Karhu, K., Fritze, H., and Liski, J.: Heterotrophic soil respiration - Comparison of different models describing its temperature dependence, Ecological Modelling, 211, 182 – 190, https://doi.org/10.1016/j.ecolmodel.2007.09.003, 2008.

Tuomi, M., Thum, T., Järvinen, H., Fronzek, S., Berg, B., Harmon, M., Trofymow, J., Sevanto, S., and Liski, J.: Leaf litter decomposition - Estimates of global variability based on Yasso07 model, Ecological Modelling, 220, 3362 – 3371, https://doi.org/10.1016/j.ecolmodel.2009.05.016, 2009.

Tuomi, M., Laiho, R., Repo, A., and Liski, J.: Wood decomposition model for boreal forests, Ecological Modelling, 222, 709 – 718, https://doi.org/10.1016/j.ecolmodel.2010.10.025, 2011.

Williams, J. W.: Variations in tree cover in North America since the last glacial maximum, Global and Planetary Change, 35, 1–23, https://doi.org/10.1016/S0921-8181(02)00088-7, 2003.

Zhou, W., Leung, L. R., and Lu, J.: Steady threefold Arctic amplification of externally forcedwarming masked by natural variability, Nature Geoscience, 17, 508–515, https://doi.org/10.1038/s41561-024-01441-1, 2024.